THE JOURNAL OF PHYSICAL CHEMISTRY C

Article

Cite This: J. Phys. Chem. C 2020, 124, 2213−2218

pubs.acs.org/JPCC

Computed Atomic Force Microscopy Images of Chromosomes by Calculating Forces with Oscillating Probes

Takashi Sumikama,*[,†] Adam. S. Foster,[†,§,∥] and Takeshi Fukuma*[,†,‡]

[†]Nano Life Science Institute (WPI-NanoLSI) and [‡]Division of Electrical Engineering and Computer Science, Kanazawa University, Kanazawa 920-1192, Japan

[§]Department of Applied Physics, Aalto University, Aalto 00076, Finland

[∥]Graduate School Materials Science in Mainz, Mainz 55128, Germany

Supporting Information

ABSTRACT: Atomic force microscopy (AFM) is a promising tool to visualize biomolecules at the sub-nanometer scale. Experimentally obtained AFM images have been compared with the simulated ones; however, such conventional images of biomolecules were usually computed by calculating equidistance surface from given atomic positions, not by calculating force. Here, we use a polymer model of a chromosome, as a representative biomolecule, and the AFM probe, and computed isoforce surfaces upon the fiber. The oscillation of probes utilized in the dynamic mode of AFM measurements was also implemented in the simulation. The computed isoforce images were clearer than the conventional equidistance ones, and a very similar images to isoforce ones were obtained when the diameter of the probe was reduced to approximately 30% in the equidistance images. Thus, the probe was found to approach very close to samples beyond the estimation of the equidistance surface, contributing clear AFM images.

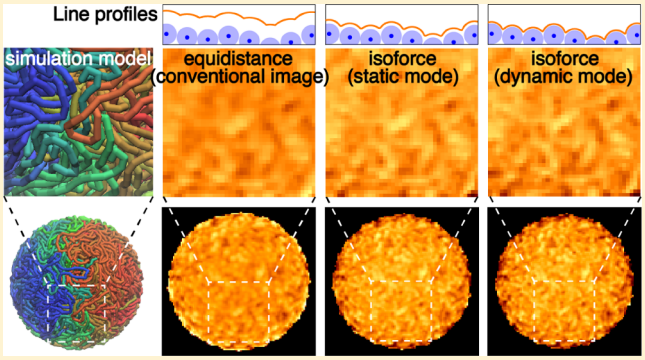

1. INTRODUCTION

Atomic force microscopy (AFM) has been extensively utilized to visualize molecules at the atomic scale.[1] This technology was originally designed to observe relatively hard materials[2] but is now applied to soft materials such as biomolecules. Especially, since the high-speed atomic force microscopy was developed,[3] various movies of biomolecular motions have been filmed.[4−8] Meanwhile, owing to the development of frequency modulation AFM (FM-AFM) for liquid environment applications, molecules are resolved at the sub-nanometer scale even in the liquid environment.[9−12]

Simulations of AFM images and comparison of them with the measurements are essential for revealing what is really resolved.[5,7,11,13−29] For simple systems, sophisticated calculations such as density functional theory[14−17,19,21] or classical molecular dynamics simulation[13,20] were employed to compute simulated AFM images, in which constant frequency shift or amplitude surfaces from samples were computed. These simulated surfaces correspond to actual topographic images by AFM measurements. On the other hand, for complicated biomolecular systems, simulated AFM images were computed by geometrically drawing equidistance surface from samples.[5,7,11,18,22,23,27] However, predictions based on an equidistant surface differ from actual AFM topographic images. Indeed, the shape of biomolecules in the simulated images were usually unnaturally rounded,[7,11,18,22−24,27] and the size of molecules did not match to the actual AFM images unless the size of the probe in simulation was smaller (about 2−50%) than that used in experiments.[5,22,23] In addition, the effect of deformation of samples by the tip−sample interaction force is not accounted for in the equidistance surface simulations. Even though some of the previous equidistance surface simulations successfully reproduced the experimentally obtained AFM images of the biomolecules, a theoretical background to support the validity of using such a small probe size should be clarified.

In this paper, we developed a method to compute isoforce surface around biomolecules with and without probe oscillation. These two cases respectively correspond to static and dynamic mode measurements.[1] In this study, we consider topographic images as isoforce surfaces to approximate both FM-AFM and the amplitude modulation AFM images. Strictly speaking, the isoforce surfaces are different from the constant frequency shift or amplitude surfaces. However, they can be more easily calculated and are good enough to reproduce the experimentally obtained AFM images with a realistic probe size by taking into account the sample deformation. Isoforce surface images of chromosome, a representative biopolymer, were simulated by employing a polymer model,[30] and were compared with conventional equidistance surface images. An

Received: October 31, 2019
Revised: December 16, 2019
Published: December 16, 2019

DOI: 10.1021/acs.jpcc.9b10263
J. Phys. Chem. C 2020, 124, 2213−2218

analysis on the computed images of the dynamic mode clarified why clear images were obtained in this mode even with a relatively blunt tip.

2. METHODS

2.1. Chromosome Polymer Model. A polymer simulation based on the bead−spring model mimicking 30 nm chromatin fibers was employed. The system comprised of one polymer consisting of 15873 beads, which corresponded to the shortest chromosome (#21) in human.[31] All the parameters of the model were the same as those in previous work.[31] In ref 31, it was written that 120 000 τ_{LJ} (the Lennard-Jones time) corresponds to 7 h in real time and $\tau_{LJ} = \sigma(m/\varepsilon)^{1/2}$, where σ and ε are the Lennard-Jones parameters and m is the mass of beads. Putting $\varepsilon = k_BT$ (k_B is the Boltzmann constant and T is the temperature) and σ = 30 nm, m was estimated to be approximately 0.2 mg. Accordingly, m = 0.2 mg was used in our study. Note that this is not an actual mass of the relevant part of chromosome, but an effective mass of them accounting also for viscosity. The Langevin equation of motion was solved to evolve the time with a time step of 10 μs, which corresponds to approximately 0.000048 τ_{LJ}. The temperature was set to 300 K.

A fractal form of the chromosome, representing the chromosome in the interphase, was made in accordance with the previous papers.[32,33] First, a starting configuration of the polymer was produced by the self-avoiding random walk in three-dimensional (3D) space.[32] Then, the following potential, previously developed, was applied to each bead in the polymer to make a compact form of chromosome[33]

$$U_{compact} = s_{pack} k_B T \, e^{(R-R_0)/s}$$

where s_{pack}, R, R_0, and s are the scaling factor to pack the polymer, the distance of beads from the center of the polymer, $0.7R_{max}$ (R_{max}, the maximum of R), and $R_0/6$, respectively.[33] Here, s_{pack} was 3. Within 200 000 steps of simulation, a fractal form was generated. The resultant structure of the compact chromosome had a diameter of ∼0.92 μm.

2.2. Model for AFM Probe. An AFM probe was modeled by the same polymer model as the chromosome assuming the probe has a diameter of 30 nm. A probe is comprised of 100 beads linearly lined with a separation of 28.8 nm (at which distance the energy is in its minimum in this model). Hence, the length of the probe is 2.88 μm. The geometry of the beads in probe was fixed in the simulation, since the AFM probe was assumed to be much more rigid than the chromosome.

The interaction between the chromosome and probe was described by the same interaction with that between beads that are not adjacent in the chromosome as a first approximation; that is, the repulsive Lennard-Jones potential

$$U_{probe} = \begin{cases} \sum_{i,j} 4k_BT[(\sigma_p/r_{ij})^{12} - (\sigma_p/r_{ij})^6 + 1/4] & \text{if } r_{ij} \le 2^{1/6}\sigma_p \\ 0 & \text{otherwise} \end{cases}$$

where r_{ij} is the distance between the beads in chromosome and those in the probe, and i runs all the beads in chromosome and j runs all the beads in probe. The σ_p is $r_{probe} + r_{sample}$. The value of r_{probe} was set to be equal to r_{sample} (that is, $r_{probe} = r_{sample}$ = 15 nm) unless otherwise noted.

The other choice of $U_{attract}$ (usual Lennard-Jones potential) was also examined.

$$U_{attract} = \sum_{i,j} 40k_BT[(\sigma_p/r_{ij})^{12} - (\sigma_p/r_{ij})^6]$$

2.3. Scanning Motion of the Probe and the Way to Compute the Topography. A tip of the probe was initially positioned apart from the center of the chromosome by 0.6 μm (z_0). The center of the chromosome was positioned to the origin (see Figure 1). All the beads in the probe were moved in the z-direction to simulate the scanning motion in the AFM measurements according to the following equation (Movie S1)

$$z = -v_{scan}t + z_0 + A \sin \omega t$$

where z, v_{scan}, t, A, and ω are the z-coordinate of the tip, the scanning velocity, time, the amplitude of the oscillation, and the frequency of the oscillation, respectively. The third term in the equation accounts for the vibration of probe. The amplitude or frequency modulation was not considered here, but the force between probe and sample was directly calculated from the derivative of U_{probe}. The scanning or approaching velocity (v_{scan}) of the probe was set to 10 μm/s, which is of the same order as experiments. A was 15 nm, corresponding to the radius of the beads in the chromosome. ω was set to 1 MHz, using the simulation time step of 0.1 μs for the probe. To set the time steps for the chromosome and probe differently, the RESPA algorithm was employed.[34]

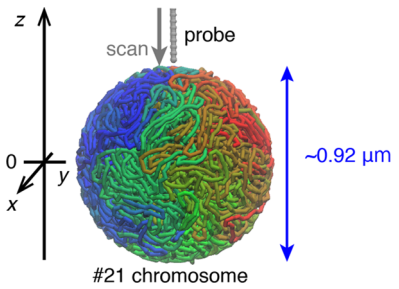

Figure 1. Simulation system and the definition of coordinate. There is one polymer composed of 15 873 beads (mimicking #21 chromosome in the interphase in a human) and one probe composed of 100 beads in the system. The chromosomal fiber is colored from red (one end) to blue (the other end). Only a part of probe was shown for clarity.

Topographies were generated by recording z-coordinates (or heights; H) of the probe tip during scanning, while changing the initial x- and y-positions of the probe by 10 nm; hence, the resolution in both directions was 10 nm. The recorded surface of $H(x, y)$ gives the topography that corresponds to the experimentally obtained AFM measurement images. Scanned area was 1 μm × 1 μm, so the number of pixels in an image was 101 × 101. The minimum resolution of the z-direction is determined by the product of the scanning velocity and the time step for the probe; here, the resolution is 10 μm/s × 0.1 μs = 0.01 Å.

In this paper, three kinds of recording were examined. First, conventional equidistant images of biomolecules were generated by recording the z-coordinates when the tip of the probe gets close to the beads of the chromosome within σ_p, which draws the equidistance surface from the polymer. In this simulation, the motion of the chromosome was fixed, in accordance with the previous computation of AFM images of biomolecules. Second, images corresponding to the dynamic

DOI: 10.1021/acs.jpcc.9b10263
J. Phys. Chem. C 2020, 124, 2213−2218

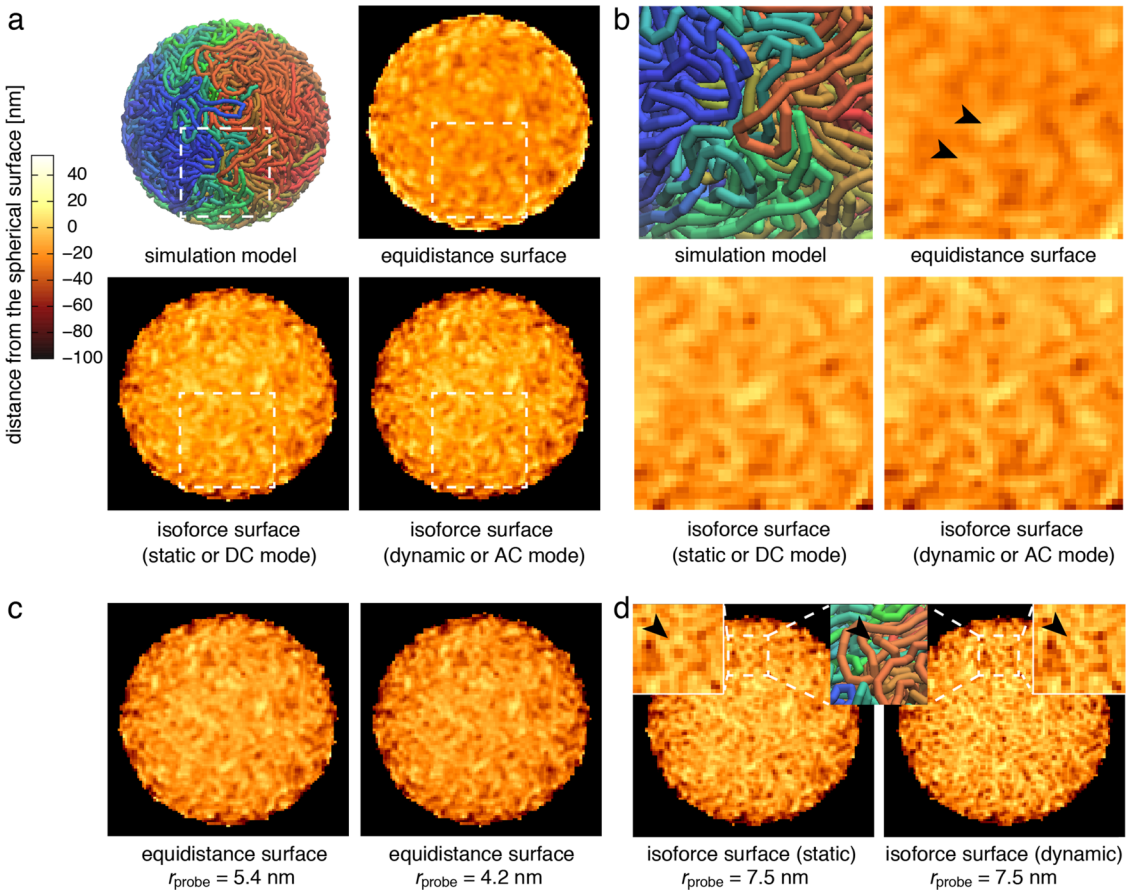

Figure 2. Simulated model and computed AFM images. (a) Whole views. Top left is a top view of Figure 1. In the computed AFM images, the height difference from the surface of a sphere having a diameter of 0.92 μm was plotted to clearly see the concavity and convexity of the surface. The equidistance surface was shifted by −20 nm to adjust its contrast with those of the isoforce surfaces. Scanned areas were 1 μm × 1 μm with 101 × 101 pixels. The radius of the probe (r_{probe}) was 15 nm. (b) Magnified views of squares in (a). Scanned areas were 0.4 μm × 0.4 μm. (c) Equidistance surface images when the radius of the probe was reduced. (d) Isoforce surface images in the static and dynamic modes when the probe size was reduced to half. The images in static and dynamic modes were shifted by +10 and +20 nm to adjust their contrasts, respectively. The enlarged views are indicated as insets. The polymer model corresponding to the relevant region is also shown.

(or AC) mode of the AFM measurements were obtained by recording the heights when the averaged forces along the z-coordinate acting on all the beads in the probe within the 10 μs exceed a setpoint, in which the sampling rate was set to be 100 kHz (Movie S2). Here, a setpoint of 100 pN, a typical value for the AFM measurements of biological molecules,[35] was employed. Lastly, AFM images of static (or DC) mode were computed by setting the amplitude (A) to zero, which removes the third term. The way to calculate AFM images in the static mode is similar to that of previous studies.[36] While computing the AFM images in dynamic and static modes, the chromosome was free to move.

All the codes to simulate AFM images were developed by ourselves. Using single core of CPU at a supercomputer of the Institute for Molecular Science in Japan (Intel Xeon Gold 2.4GHz), computing time to obtain a height information at one position was ∼0.1 s (equidistance estimation), ∼65 s (in the static mode), and ∼135 s (in the dynamic mode). All the snapshots and movies were produced using the Visual Molecular Dynamics package.[37]

3. RESULTS

The simulation system has a single fiber mimicking #21 chromosome, the shortest chromosome in a human, and one probe (Figure 1). The chromosome was constrained in a sphere to mimic its structure in the interphase.[38] The probe was scanned in the z-direction at each xy-position to approach the chromosome (Movie S1). This corresponds to the scanning motion in the AFM measurements.

Three kinds of AFM image were computed (Figure 2a,b). First, in accordance with the conventional geometrically estimated AFM images of biomolecules,[5,7,11,18,22,23,27] an equidistant surface from the chromosome was drawn (top right in Figure 2a). In this image, many bumps were seen, whose shapes are mostly rounded. These rounded shapes were, as mentioned, typically seen in the computed AFM images of biomolecules.[7,11,18,22−24,27] Because of this roundness, the overall view is somehow blurred; thus, it is difficult to distinguish fibers except for some fiberlike structures in the magnified view (arrowheads in the top right of Figure 2b).

Two kinds of isoforce surface-simulating static and dynamic modes were computed. In the static mode, heights (or z-coordinates) of the tip were recorded when the instantaneous force that the probe feels exceeds a certain force (the so-called setpoint). The setpoint was set to be 100 pN, a typical value for biomolecular measurements.[35] In the dynamic mode, the detected force was defined as the time averaged force of the instantaneous forces in the sampling time (in this case, 10 μs;

DOI: 10.1021/acs.jpcc.9b10263
J. Phys. Chem. C 2020, 124, 2213−2218

being equivalent to 10 cycles of oscillation and 100 time steps of numerical integration) (Movie S2). In these simulations, the sample (here chromosome) was free to move to account for its deformation by the tip−sample interaction force in the AFM measurements unlike the previous equidistance surface simulations. Computed isoforce surfaces in both static and dynamic modes were sharper than the equidistance surface (bottoms in Figure 2a). Although these two isoforce surface images look similar, there is a difference when the probe size was reduced, as shown later. In contrast to the equidistance surface image, the fibers of the chromosome were resolved in the isoforce surface images. In the magnified views (bottoms in Figure 2b), fibers are observed whose shapes were close to those in the simulation model (top left in Figure 2b).

In the previous papers, it was shown that the most similar images to the experimentally measured AFM images were obtained when the probe size was reduced to 2−50%.[5,22,23] One hundred different equidistance surface images were computed while changing probe size from 1 to 100%. It was found that the most similar image with the isoforce surface in the static mode was obtained when the radius of the probe (r_{probe}) was reduced to 36% (r_{probe} = 5.4 nm) and that in dynamic mode this was observed when r_{probe} was 4.2 nm (28%) (see the quantitative estimation of difference between images; Figure S1). The resultant equidistance surfaces (r_{probe} = 5.4 nm (36%) and 4.2 nm (28%)) are indicated in Figure 2c. These images were different from the original equidistance surface (r_{probe} = 15 nm; top right in Figure 2a) but similar to the isoforce surface images. As a result, fibers were resolved in these images. This means that it is important to reduce the tip radius to approximately 30% of that actually used in the AFM measurements to gain the best fit of computed AFM images with the corresponding AFM measurements, rationalizing the use of reduced tip size while simulating the AFM images.[5,22,23] More importantly, these results signify that the probe approaches closer to the sample than expected from the probe size in the AFM measurements, as though the probe had smaller size than its real size.

Also, it is widely considered that higher-resolution images are provided when a smaller sized or sharpened tip is used. Isoforce surfaces in the static and dynamic modes were computed when r_{probe} was reduced by half, i.e., r_{probe} = 7.5 nm (Figure 2d). Two images in both modes were of higher resolution than those of the original tip size: further, fibers are clearly seen. At this probe size, the image in the dynamic mode is slightly finer than that in the static mode. Especially, fibers in the inset (arrowheads) were not separated in the view of static mode, but they were discriminated in the dynamic mode image. Thus, our results show that the simulated AFM images in the dynamic mode are sharper than those in the static mode.

One may think that the flexibility of the sample increased the resolution; for example, the separated view of the two fibers (right inset in Figure 2d) is considered to be a result of a displacement of these fibers to make a cleft between them while the oscillating probe approaches. To clarify whether this is correct or not, isoforce surfaces in the static and dynamic modes while completely fixing fibers were computed (Figure S2). The obtained images were almost the same as the original images in the case where the fibers were free to move irrespective of the scanning mode and probe size, except for a slight height difference (∼1 nm). Accordingly, the flexibility has little effect on the increase of resolution because of the much slower motion of chromosomal fiber compared to the approaching probe (Movie S1).[39] Moreover, to investigate the influence of attractive force between probe and sample, AMF images with the probe−sample attraction were also simulated using $U_{attract}$ (Figure S3). The resultant topographies were somewhat blurred but mostly similar to those obtained using the repulsive Lennard-Jones potential (Figure S3). This means that the attraction term has little effect on the topographic images.

In the line profiles, the difference among the equidistance and isoforce surfaces was clearly confirmed (Figure 3). The

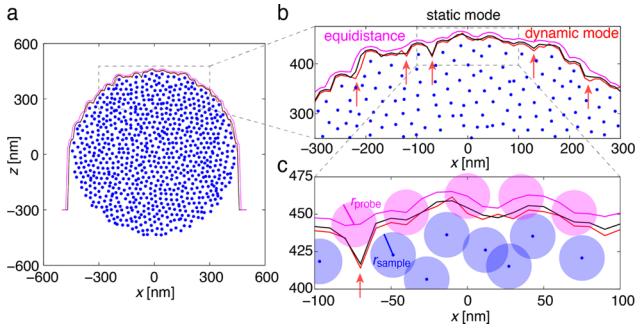

Figure 3. Line profiles of equidistance and isoforce surfaces along a cross section cutting the chromosome at the center. (a) A whole picture. (b) Enlarged view of (a). (c) Enlarged view of (b). Blue dots show the positions of beads constituting chromosome within a slab of 15 nm from the cross section. Red arrows indicate the positions where the isoforce curves intrude into the sample. Magenta and blue circles in bottom right show the radius of the probe (r_{probe}) and the beads in the sample (r_{sample}), respectively. Here, r_{probe} = r_{sample} = 15 nm.

line profile of the equidistance curve (magenta in Figure 3) effectively follows the radius (r_{sample} + r_{probe}) of a circle (or sphere for three-dimensional (3D) space), such that the line is rounded in the 2D line profile, and results in round bumps in the equidistance surface in 3D space (top right in Figure 2a).

By contrast, the isoforce curves (black lines in Figure 3 for static mode, and red for dynamic mode) were rugged and zigzag. Hence, they are qualitatively different from the equidistance curve. This zigzag or indented curve contributes not only to increase the resolution in the height direction but also to a separated view of the fibers. The isoforce curves in both modes run closer to the beads than the equidistant curve. Again, this means that the probes come close to the samples in the actual AFM measurements, which is in accordance with the motivation of the FM-AFM.[1] In addition, at some points, we can see that the isoforce curves deeply intrude into the chromosome (red arrows, Figure 3b,c). A remarkable example is shown in Figure 3c: the equidistance curve runs over two leftmost beads of chromosome, while the isoforce curves indent and make a cleft between them. It shows that the equidistance curve cannot separate these two beads, while the isoforce curves can really resolve them. Thus, these intrusions are responsible for the fine resolution.

Finally, it is important to quantitatively clarify to what extent the probe can approach the sample. Conventional simulated AFM images of biomolecules are, as noted, based on equidistance surfaces. On this surface, the force in our model is only 3.3 pN. Generally, the force on the equidistance surface is given by $24\varepsilon/\sigma$, where ε and σ are the usual parameters in a Lennard-Jones potential. For example, $24\varepsilon/\sigma$ is 81.8 pN for the SPC/E water model and 42.2 pN for sp^2 carbon atom in the AMBER force field.[40,41] Note that the z-component of force is

DOI: 10.1021/acs.jpcc.9b10263
J. Phys. Chem. C 2020, 124, 2213−2218

always smaller than these values. The force values are thus smaller than the usual setpoint (100 pN); accordingly, the probe approaches toward the sample beyond the equidistance surface against the repulsive force from the sample even in the static mode because of setpoint.[42]

In the dynamic mode, the probe is oscillating and the detection force is a time average of the instantaneous force between the probe and sample (Movie S2). Thus, the tip−sample repulsion is weakened by the broad distribution of the tip in oscillation: strong repulsion when the tip approaches the sample is averaged by the weak (or nearly zero) repulsion when the tip is far from the sample in its oscillation cycle. Even though the detecting force is below 100 pN, the instantaneous force is close to 500 pN (Movie S2). It approaches approximately 790 pN when the motion of sample was fixed (hence, the probe stopped at slightly higher positions in Figure S2). Accordingly, the oscillating probe can approach closer to samples than in the static mode, and the deformation of sample allows the probe to get even closer. This demonstrates why the isoforce curve in the dynamic mode runs closer to the sample compared to that in the static mode (Figure 3). As a result, the probe gets closer to the sample in the AFM measurements beyond the simple expectation from the equidistance surface.

4. CONCLUSIONS

We computed the isoforce surface in both the static and dynamic modes of polymers modeling a chromosome and AFM probe. It was found that the isoforce surface was clearer than the equidistance surface (conventional simulated AFM images of biomolecules) due to deep indentation; the tip can closely approach the sample beyond the equidistance surface against the tip−sample repulsion.[42] In previous studies, an unrealistically small probe size was assumed in the equidistance surface simulation to reproduce the resolution of the real AFM images.[5,22,23] Here, we have provided a theoretical explanation of why such a small probe size was necessary and how it can improve the similarity between equidistance surface images and real AFM images. We have also demonstrated that this problem can be solved using an isoforce surface simulation. In addition, we clarified the approximately 3-fold difference between the probe sizes used in the real experiments and equidistance surface simulation. This quantitative understanding may allow us to estimate the size of the experimentally used probe by comparison between the AFM images obtained in experiments and simulation.

■ ASSOCIATED CONTENT

Supporting Information

The Supporting Information is available free of charge at https://pubs.acs.org/doi/10.1021/acs.jpcc.9b10263.

Movie of probe approaching S1 (Movie S1)

Movie of oscillating probe and a force meter S2 (Movie S2)

Difference between the equidistance and isoforce surface images (Figure S1); isoforce surface images when the motion of chromosomes was completely fixed (Figure S2); isoforce surface images with attraction between probe and chromosome (Figure S3) (PDF)

■ AUTHOR INFORMATION

Corresponding Authors

*E-mail: sumi@staff.kanazawa-u.ac.jp (T.S.).
*E-mail: fukuma@staff.kanazawa-u.ac.jp (T.F.).

ORCID

Takashi Sumikama: 0000-0003-3696-5720
Adam. S. Foster: 0000-0001-5371-5905
Takeshi Fukuma: 0000-0001-8971-6002

Notes

The authors declare no competing financial interest.

■ ACKNOWLEDGMENTS

This work was partially supported by a Grant-in-Aid for Young Scientists (No. 17K17768), PRESTO from JST Japan (JPMJPR19KC), Grant-in-Aid for Scientific Research (No. 16H02111), WPI-NanoLSI Transdisciplinary Research Promotion Grant from Kanazawa University, and JST-Mirai Program (No. 18077272). The calculation was carried out on the supercomputers at the Research Center for Computational Science in Okazaki, Japan. T.S. is grateful to Prof. Uchihashi (Nagoya Univ.), Dr. Miyashita (Riken), Dr. Yurtsever (Kanazawa Univ.), Dr. Miyazawa (Kanazawa Univ.), and Dr. Sumino (Kanazawa Univ.) for fruitful discussion.

■ REFERENCES

(1) *Noncontact Atomic Force Microscopy*; Morita, S.; Wiesendanger, R.; Meyer, E., Eds.; Springer, 2002.
(2) Binnig, G.; Quate, C. F.; Gerber, Ch. Atomic Force Microscope. *Phys. Rev. Lett.* **1986**, *56*, 930−933.
(3) Ando, T.; Kodera, N.; Takai, E.; Maruyama, D.; Saito, K.; Toda, A. A High-Speed Atomic Force Microscope for Studying Biological Macromolecules. *Proc. Natl. Acad. Sci. U.S.A.* **2001**, *98*, 12468−12472.
(4) Kodera, N.; Yamamoto, D.; Ishikawa, R.; Ando, T. Video Imaging of Walking Myosin V by High-Speed Atomic Force Microscopy. *Nature* **2010**, *468*, 72−76.
(5) Uchihashi, T.; Iino, R.; Ando, T.; Noji, H. High-Speed Atomic Force Microscopy Reveals Rotary Catalysis of Rotorless F1-ATPase. *Science* **2011**, *333*, 755−758.
(6) Ruan, Y.; Miyagi, A.; Wang, X.; Chami, M.; Boudker, O.; Scheuring, S. Direct Visualization of Glutamate Transporter Elevator Mechanism by High-Speed AFM. *Proc. Natl. Acad. Sci. U.S.A.* **2017**, *114*, 1584−1588.
(7) Mori, T.; Sugiyama, S.; Byrne, M.; Johnson, C. H.; Uchihashi, T.; Ando, T. Revealing Circadian Mechanisms of Integration and Resilience by Visualizing Clock Proteins Working in Real Time. *Nat. Commun.* **2018**, *9*, No. 3245.
(8) Sumino, A.; Sumikama, T.; Uchihashi, T.; Oiki, S. High-Speed AFM Reveals Accelerated Binding of Agitoxin-2 to a K^+ Channel by Induced Fit. *Sci. Adv.* **2019**, *5*, No. eaax0495.
(9) Fukuma, T.; Kimura, M.; Kobayashi, K.; Matsushige, K.; Yamada, H. Dependent of Low Noise Cantilever Deflection Sensor for Multi Environment Frequency-Modulation Atomic Force Microscopy. *Rev. Sci. Instrum.* **2005**, *76*, No. 053704.
(10) Asakawa, H.; Ikegami, K.; Setou, M.; Watanabe, N.; Tsukada, M.; Fukuma, T. Submolecular-Scale Imaging of α-Helices and C-Terminal Domain of Tubulins by Frequency Modulation Atomic Force Microscopy in Liquid. *Biophys. J.* **2011**, *101*, 1270−1276.
(11) Ido, S.; Kimiya, H.; Kobayashi, K.; Kominami, H.; Matsushige, K.; Yamada, H. Immunoactive Two-Dimensional Self-Assembly of Monoclonal Antibodies in Aqueous Solution Revealed by Atomic Force Microscopy. *Nat. Mater.* **2014**, *13*, 264−270.
(12) Kuchuk, K.; Sivan, U. Hydration Structure of a Single DNA Molecule Revealed by Frequency-Modulation Atomic Force Microscopy. *Nano Lett.* **2018**, *18*, 2733−2737.

DOI: 10.1021/acs.jpcc.9b10263
J. Phys. Chem. C 2020, 124, 2213−2218

(13) Fukuma, T.; Reischl, B.; Kobayashi, N.; Spijker, P.; Canova, F. F.; Miyazawa, K.; Foster, A. S. Mechanism of Atomic Force Microscopy Imaging of Three-Dimensional Hydration Structures at a Solid-Liquid Interface. *Phys. Rev. B* **2015**, *92*, No. 155412.
(14) Emmrich, M.; Huber, F.; Pielmeier, F.; Welker, J.; Hofmann, T.; Schneiderbauer, M.; Meuer, D.; Polesya, S.; Mankovsky, S.; Ködderitzsch, D.; et al. Subatomic Resolution Force Microscopy Reveals Internal Structure and Adsorption Sites of Small Iron Clusters. *Science* **2015**, *348*, 308−311.
(15) Sakai, Y.; Lee, A. J.; Chelikowsky, J. R. First-Principle Atomic Force Microscopy Image Simulations with Density Embedding Theory. *Nano Lett.* **2016**, *16*, 3242−3246.
(16) Miyata, K.; Tracy, J.; Miyazawa, K.; Haapasilta, V.; Spijker, P.; Kawagoe, Y.; Foster, A. S.; Tsukamoto, K.; Fukuma, T. Dissolution Processes at Step Edges of Calcite in Water Investigated by High-Speed Atomic Force Microscopy and Simulation. *Nano Lett.* **2017**, *17*, 4083−4089.
(17) Asakawa, H.; Holmström, E.; Foster, A. S.; Kamimura, S.; Ohno, T.; Fukuma, T. Direct Imaging of Atomic-Scale Surface Structures of Brookite TiO_2 Nanoparticles by Frequency Modulation Atomic Force Microscopy in Liquid. *J. Phys. Chem. C* **2018**, *122*, 24085−24093.
(18) Bose, K.; Lech, C. J.; Heddi, B.; Phan, A. T. High-Resolution AFM Structure of DNA G-Wires in Aqueous Solution. *Nat. Commun.* **2018**, *9*, No. 1959.
(19) Peng, J.; Cao, D.; He, Z.; Guo, J.; Hapala, P.; Ma, R.; Cheng, B.; Chen, J.; Xie, W. J.; Li, X.-Z.; et al. The Effect of Hydration Number on the Interfacial Transport of Sodium Ions. *Nature* **2018**, *557*, 701−705.
(20) Reischl, B.; Raiteri, P.; Gale, J. D.; Rohl, A. L. Atomistic Simulation of Atomic Force Microscopy Imaging of Hydration Layers on Calcite, Dolomite, and Magnesite Surfaces. *J. Phys. Chem. C* **2019**, *123*, 14985−14992.
(21) Miyata, K.; Kawagoe, Y.; Tracy, J.; Miyazawa, K.; Foster, A. S.; Fukuma, T. Variations in Atomic-Scale Step Edge Structures and Dynamics of Dissolving Calcite in Water Revealed by High-Speed Frequency Modulation Atomic Force Microscopy. *J. Phys. Chem. C* **2019**, *123*, 19786−19793.
(22) Rodriguez-Ramos, J.; Perrino, A. P.; Garcia, R. Dependence of the Volume of an Antibody on the Force Applied in a Force Microscopy Experiment in Liquid. *Ultramicroscopy* **2016**, *171*, 153−157.
(23) Kozai, T.; Sekiguchi, T.; Satoh, T.; Yagi, H.; Kato, K.; Uchihashi, T. Two-Step Process for Disassembly Mechanism of Proteasome α7 Homo-Tetradecamer by α6 Revealed by High-Speed Atomic Force Microscopy. *Sci. Rep.* **2017**, *7*, No. 15373.
(24) Yamada, H.; Kobayashi, K.; Fukuma, T.; Hirata, Y.; Kajita, T.; Matsushige, K. Molecular Resolution Imaging of Protein Molecules in Liquid Using Frequency Modulation Atomic Force Microscopy. *Appl. Phys. Express* **2009**, *2*, No. 095007.
(25) Philippsen, A.; Im, W.; Engel, A.; Schirmer, T.; Roux, B.; Müller, D. J. Imaging the Electrostatic Potential of Transmembrane Channels: Atomic Probe Microscopy of OmpF Porin. *Biophys. J.* **2002**, *82*, 1667−1676.
(26) Scheuring, S.; Buzhynskyy, N.; Jaroslawski, S.; Pedro Gonçalves, R.; Hite, R. K.; Walz, T. Structural Models of the Supramolecular Organization of AQP0 and Connexons in Junctional Microdomains. *J. Struct. Biol.* **2007**, *160*, 385−394.
(27) Trinh, M.-H.; Odorico, M.; Pique, M. E.; Teulon, J.-M.; Roberts, V. A.; Ten Eyck, L. F.; Getzoff, E. D.; Parot, P.; Chen, S.-W. W.; Pellequer, J.-L. Computational Reconstruction of Multidomain Proteins Using Atomic Force Microscopy Data. *Structure* **2012**, *20*, 113−120.
(28) Chen, S.-W. W.; Odorico, M.; Meillan, M.; Vellutini, L.; Teulon, J.-M.; Parot, P.; Bennetau, B.; Pellequer, J.-L. Nanoscale Structural Features Determined by AFM for Single Virus Particles. *Nanoscale* **2013**, *5*, 10877−10886.
(29) He, J.; Wang, J.; Hu, J.; Sun, J.; Czajkowsky, D. M.; Shao, Z. Single Molecule Atomic Force Microscopy of Aerolysin Pore Complexes Reveals Unexpected Star-Shaped Topography. *J. Mol. Recogn.* **2015**, *29*, 174−181.
(30) Phillips, R.; Kondev, J.; Theriot, J.; Garcia, H.et al. *Physical Biology of the Cell*; Gerland Science, 2012.
(31) Di Stefano, M.; Paulsen, J.; Lien, T. G.; Hovig, E.; Micheletti, C. Hi-C-Constrained Physical Models of Human Chromosomes Recover Functionally-Related Properties of Genome Organization. *Sci. Rep.* **2016**, *6*, No. 35985.
(32) Le, T. B. K.; Imakaev, M. V.; Mirny, L. A.; Laub, M. T. High-Resolution Mapping of the Spatial Organization of a Bacterial Chromosome. *Science* **2013**, *342*, 731−734.
(33) Lieberman-Aiden, E.; van Berkum, N. L.; Williams, L.; Imakaev, M.; Ragoczy, T.; Telling, A.; Amit, I.; Lajoie, B. R.; Sabo, P. J.; Dorschner, M. O.; et al. Comprehensive Mapping of Long-Range Interactions Reveals Folding Principles of the Human Genome. *Science* **2009**, *326*, 289−293.
(34) Tuckerman, M.; Berne, B. J.; Martyna, G. J. Reversible Multiple Time Scale Molecular Dynamics. *J. Chem. Phys.* **1992**, *97*, 1900−2001.
(35) Müller, D. J.; Fotiadis, D.; Scheuring, S.; Müller, S. A.; Engel, A. Electrostatically Balanced Subnanometer Imaging of Biological Specimens by Atomic Force Microscope. *Biophys. J.* **1999**, *76*, 1101−1111.
(36) Hapala, P.; Kichin, G.; Wagner, C.; Tautz, F. S.; Temirov, R.; Jelínek, P. Mechanism of High-Resolution STM/AFM Imaging with Functionalized Tips. *Phys. Rev. B* **2014**, *90*, No. 085421.
(37) Humphrey, W.; Dalke, A.; Schulten, K. VMD: Visual Molecular Dynamics. *J. Mol. Graphics* **1996**, *14*, 33−38.
(38) Naumova, N.; Imakaev, M.; Fudenberg, G.; Zhan, Y.; Lajoie, B. R.; Mirny, L. A.; Dekker, J. Organization of the Mitotic Chromosome. *Science* **2013**, *342*, 948−953.
(39) Nozaki, T.; Imai, R.; Tanbo, M.; Nagashima, R.; Tamura, S.; Tani, T.; Joti, Y.; Tomita, M.; Hibino, K.; Kanemaki, M. T.; et al. Dynamic Organization of Chromatin Domains Revealed by Super-Resolution Live-Cell Imaging. *Mol. Cell* **2017**, *67*, 282−293.
(40) Berendsen, H. J. C.; Grigera, J. R.; Straatsma, T. R. The Missing Term in Effective Pair Potentials. *J. Phys. Chem. A* **1987**, *91*, 6269−6271.
(41) Cornell, W. D.; Cieplak, P.; Bayly, C. I.; Gould, I. R., Jr; Merz, K. M.; Ferguson, D. M.; Spellmeyer, D. C.; Fox, T.; Caldwell, J. W.; Kollman, P. A. A Second Generation Force Field for the Simulation of Proteins, Nucleic Acids, and Organic Molecules. *J. Am. Chem. Soc.* **1995**, *117*, 5179−5197.
(42) Sokolov, I. Yu.; Henderson, G. S.; Wicks, F. J. Pseudo-Non-Contact AFM Imaging? *Appl. Surf. Sci.* **1999**, *140*, 362−365.

DOI: 10.1021/acs.jpcc.9b10263
J. Phys. Chem. C 2020, 124, 2213−2218